

1 Predicting gridded winter PM_{2.5} concentration in east of China

2 Zhicong Yin^{1,2,3*}, Mingkeng Duan¹, Yuyan Li¹, Tianbao Xu¹, Huijun Wang^{1,2,3}

3 ¹Key Laboratory of Meteorological Disaster, Ministry of Education / Joint International Research Laboratory of Climate and
4 Environment Change (ILCEC) / Collaborative Innovation Center on Forecast and Evaluation of Meteorological Disasters
5 (CIC-FEMD), Nanjing University of Information Science & Technology, Nanjing, 210044, China

6 ²Southern Marine Science and Engineering Guangdong Laboratory (Zhuhai), Zhuhai, 519080, China

7 ³Nansen-Zhu International Research Centre, Institute of Atmospheric Physics, Chinese Academy of Sciences, Beijing,
8 100029, China

9
10 **Correspondence to:* Zhicong Yin (yinzhc@nuist.edu.cn)

11
12 **Abstract.** Exposure to high levels of concentration of fine particle matters with diameter $\leq 2.5 \mu\text{m}$ (PM_{2.5}) can lead to great
13 threats to human health in east of China. Air pollution control has greatly reduced the PM_{2.5} concentration and entered a
14 crucial stage that required supports like fine seasonal prediction. In this study, we analysed the contributions of emission
15 predictors and climate variability to seasonal prediction of PM_{2.5} concentration. The socioeconomic-PM_{2.5}, isolated by
16 atmospheric chemical models, could well describe the gradual increasing trend of PM_{2.5} during the winters of 2001–2012
17 and the sharp decreasing trend since 2013. The preceding climate predictors have successfully simulated the interannual
18 variability of winter PM_{2.5} concentration. Based on the year-to-year increment approach, a model for seasonal prediction of
19 gridded winter PM_{2.5} concentration (10km \times 10km) in east of China was trained by integrating of emission and climate
20 predictors. The area-averaged percentage of same sign was 81.48% (relative to the winters of 2001–2019) in the leave-one-
21 out validation. In three densely populated and heavily polluted regions, the correlation coefficients were 0.93 (North China),
22 0.95 (Yangtze River Delta) and 0.88–0.87 (Pearl River Delta) during 2001–2019 and the root-mean-square errors were 6.58,
23 4.42 and 4.67 $\mu\text{g}/\text{m}^3$. More important, the significant decrease in PM_{2.5} concentration, resulted from implementation of
24 strict emission control measures in recent years, was also reproduced. In the recycling independent tests, the prediction
25 model developed in this study also maintained high accuracy and robustness. Furthermore, the accurate gridded PM_{2.5}
26 prediction had the potential to support air pollution control on regional and city scales.

30 **1 Introduction**

31 Exposure to fine particle matters with diameter $\leq 2.5 \mu\text{m}$ (PM_{2.5}) can lead to severe respiratory and cardiovascular
32 diseases (Cohen et al., 2017) and even directly induces DNA damages (Wu et al., 2017). According to the newly
33 recommended air quality guidelines, the level of annual mean PM_{2.5} $> 5 \mu\text{g}/\text{m}^3$ has the potential to threat human health
34 (World Health Organization, 2021). In 2020, the average PM_{2.5} concentration in cities of China was $33 \mu\text{g}/\text{m}^3$, although the
35 implementation of strict air quality control measures substantially reduced the emission of primary pollutants (Zhang et al.,
36 2022). The changes in the emission of air pollutants also resulted in the shift of winter PM_{2.5} trend in east of China, that is,
37 the winter PM_{2.5} concentration gradually increased during 2000–2012 but has been decreasing since 2013 (Figure 1a).
38 Evident interannual variation was also be found in the changes of PM_{2.5} concentration in winter (December-January-
39 February), which was largely attributed to climate variability (Yin et al., 2020a, 2020b). Given the severe impact of PM_{2.5}
40 pollution and yearly plan of control action, it is meaningful and urgent to develop prediction models to forecast PM_{2.5}
41 concentration 1~3 months in advance. Furthermore, the predicting results should have high resolution to provide valuable
42 information on the regional and city levels.

43 To accurately predict climate anomalies is still a real challenge, while predicting air pollution on seasonal scale is much
44 harder than predicting routine meteorological elements (Wang et al., 2021). In general, the methods of climate prediction
45 included numerical climate models and statistical approaches. Despite the great advances in atmospheric chemical models in
46 recent years, most of these models were not designed for real-time operation of seasonal predictions and lacked the coupling
47 of the atmospheric chemical composition and the entire earth system (An et al., 2018). Additionally, statistical prediction of
48 winter PM_{2.5} concentration was limited by the short sequences of observed atmospheric composition, because broad
49 observations only started in 2014 in China. The gray prediction model performed well in dealing with small sample data and
50 thus was used to forecast PM_{2.5} concentration (Wang and Du, 2021; Wu et al., 2019; Xiong et al., 2019). Considering the
51 strong control measures implemented to improve air quality, the buffer operators can be added to the discrete gray prediction
52 model to reduce deviations (Dun et al., 2020). These mathematical models showed certain predictive skills, but lacked of
53 underlying physical mechanisms and long-standing robustness.

54 Many previous studies employed the long-term observed visibility, air humidity and weather phenomena to reconstruct
55 data of haze (Xu et al., 2016; Zou et al., 2017; He et al., 2019; Yin et al., 2020b). The change in winter haze days consists of
56 long-term trend and interannual-decadal variations. The long-term trend of haze was mainly determined by human activities
57 (i.e., primary pollutants emission and climate change), while its interannual-decadal variations had close relationships with
58 climate variability (Yin et al., 2020b; Geng et al., 2021a). Besides analysis of climate mechanisms, the number of haze days
59 was also used as a proxy-predictand of PM_{2.5} pollution. Taking advantage of the memory effect in slow-varying climate
60 forcings (e.g., sea surface temperature and sea ice), the number of haze days was successfully predicted in North China (Yin
61 and Wang 2016; Yin et al., 2017), Yangtze River Delta (Dong et al., 2021) and Fenwei Plain (Zhao et al., 2021). Chang et al.
62 (2021) used regional stratospheric warming over northeastern Asia in November to predict haze pollution in the Sichuan

63 Basin in 5–7 weeks. Information from the preceding autumn El Niño was also extracted to predict winter haze days in South
64 China (Cheng et al., 2019) and aerosol optical depth over northern India (Gao et al., 2019). In most of these studies, the
65 predictand is area-averaged number of haze days, which was a bit different from PM_{2.5} concentration in use and fine spatial
66 information was missing.

67 The Tracking Air Pollution (TAP) database combines information from ground observations, satellite retrievals,
68 emission inventories and chemical transport model simulations based on data fusion. A full-coverage PM_{2.5} reanalysis
69 dataset with a spatial resolution of 10km×10km from 2000 until present has been released (Geng et al., 2021b). It becomes
70 feasible to develop statistical prediction model of PM_{2.5} concentration based on this long-range dataset. Furthermore, as
71 reviewed by Yin et al., (2022), the predictability of winter haze decreased ~~during after 2014–2020~~, which was mainly
72 attributed to the disturbances from super-strict emissions reduction in China. Rapid changes in human activities and changes
73 in climate anomalies both should be considered and included in PM_{2.5} prediction models. This is the major motivation of the
74 present study to build a climate-emission hybrid model for the prediction of gridded PM_{2.5} concentration in east of China.
75 The findings of this study have enormous potentials to support fine designs and implements of air pollution control in
76 advance.

77 **2 Datasets and method**

78 **2.1 Data**

79 The monthly sea ice concentration (SI) and sea surface temperature (SST) dataset [from 2000 to 2019](#), with a spatial
80 resolution of 1°×1°, were provided by the Met Office Hadley Centre (Rayner et al. 2003,
81 <https://www.metoffice.gov.uk/hadobs/hadisst/>). Monthly soil moisture (Soilw), snow depth (SD), geopotential height at
82 500hPa (Z500) and 850hPa (Z850), sea level pressure (SLP) and 10m wind were extracted from the fifth generation
83 reanalysis product (ERA5) produced by the European Center for Medium Range Weather Forecasts (Hersbach et al. 2020,
84 <https://cds.climate.copernicus.eu/#!/search?text=ERA5&type=dataset>). Annual emissions of ammonia, nitrogen oxide, BOC,
85 primary PM_{2.5}, and sulfur dioxide in China were derived from the MEIC model (<http://www.meicmodel.org/>; Li et al., 2017).

86 Hourly site-observed PM_{2.5} concentration during 2014–~~2020–2019~~ were also employed in the present study
87 (<https://www.aqistudy.cn/historydata/>). The long-term and high-resolution TAP PM_{2.5} concentration dataset during 2000–
88 ~~2020–2019~~ can be downloaded from <http://tapdata.org> (Geng et al. 2021b). The PM_{2.5} reanalysis data were used as training
89 data as well as test data in the construction of the prediction model, and the observed PM_{2.5} concentration were also applied
90 to verify the prediction skill of the model.

91 **2.2 Isolation of socioeconomic-PM_{2.5}**

92 We employed the simulated annual-mean PM_{2.5} concentrations that exclude the meteorological contributions to
93 represent the impacts of anthropogenic emissions. Compared with direct use of emission inventory of primary pollutants, the
94 isolated socioeconomic-PM_{2.5} (SE-PM_{2.5}) involved both results of emission changes and follow-up physical and chemical
95 reactions in the air. To remove the meteorological influences from the TAP PM_{2.5} data, we used chemical transport models
96 and emission inventories to separate the contributions from emission and meteorology changes. Following the approach
97 proposed by Xiao et al. (2021), we used a ‘fix emission’ scenario to quantify the impacts of interannual meteorological
98 variation on PM_{2.5} concentration in Community Multiscale Air Quality (CMAQ) model. Subsequently, a full simulation with
99 year-by-year emission and meteorology was completed. Differences between the ‘fix emission’ simulation and the full
100 simulation were considered to be PM_{2.5} concentrations driven by anthropogenic emissions. This data has been analyzed to
101 quantify relative influences of different drivers on PM_{2.5}-related deaths in China (Geng et al. 2021b).

102 **2.3 Year-to-year increment prediction**

103 The year-to-year increment approach is proposed to improve the skill of climate prediction (Wang et al., 2008), in
104 which the predicted object is not climate anomalies but is the difference between the current and the previous year (DY).
105 After adding the predicted DY to the observed predictand in the year before, the final predicted results during 2001–2019
106 were obtained. Based on full use of observations in the previous year, the gradually changing trend and inter-decadal
107 components can be well reproduced. Anthropogenic-natural-forcing predictand could be represented by $Y = YS + YC$, where
108 YS and YC denoted the slowly varying socio-economic and climatic components, respectively. In the DY approach, which
109 was expressed by:

$$110 \quad DY = Y_t - Y_{t-1} = (YS_t + YC_t) - (YS_{t-1} + YC_{t-1}) = (YS_t - YS_{t-1}) + (YC_t - YC_{t-1})$$

111 where the subscripts t and $t-1$ indicated the current and the previous years. Before 2013, the difference between
112 anthropogenic emissions in two adjacent years was small, Yin and Wang (2016) assumed $(YS_t - YS_{t-1}) \approx 0$ and proposed
113 that DY was mainly influenced by climate variability. However, due to significant reduction of anthropogenic emissions
114 after the implementation of China’s Air Pollution Prevention and Control Action Plan (Zhang and Geng, 2020), the
115 assumption of $(YS_t - YS_{t-1}) \approx 0$ was no longer completely valid. Therefore, it is meaningful to consider the information of
116 rapid emission changes and re-build the prediction model (Yin et al., 2022).

117 (1) Seasonal prediction model based on SE-PM_{2.5} (SP-SE): this prediction model unilaterally emphasized the impacts of
118 human activities and was trained by DY of SE-PM_{2.5} in each grid.

119 (2) Seasonal prediction model based on preceding climate variability (SP-CV): this prediction model was highly
120 focused on the impacts of climate condition and trained by DY of closely related climate factors.

121 (3) Seasonal prediction model based on both SE-PM_{2.5} and climate (SP-EC): the contributions of emissions and climate
122 factors are incorporated into one prediction model, i.e., combining the PM_{2.5} DY from SP-SE and SP-CV.

123 In the leave-one-out cross validation, root-mean-square error (RMSE), relative bias and correlation coefficient (CC)
124 were calculated. When discussing the CC after the detrending, the linear trend was removed by stages (i.e., winters of 2001–
125 2011 and 2012–2019). The percentage of the same sign (PSS; same sign means the mathematical sign of the fitted and
126 observed PM_{2.5} anomalies was the same) was also computed.

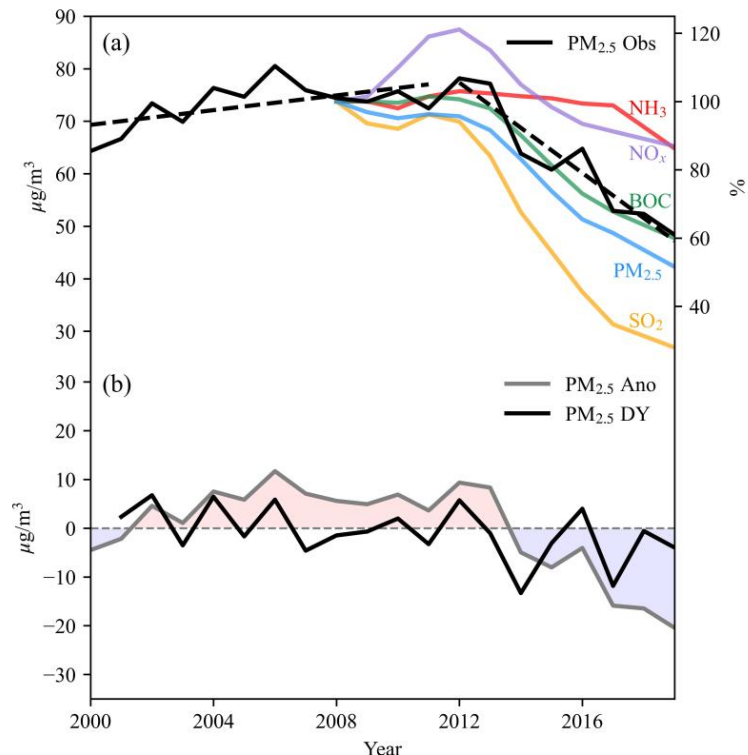
127 **3 Relative contributions of emission and climate predictors**

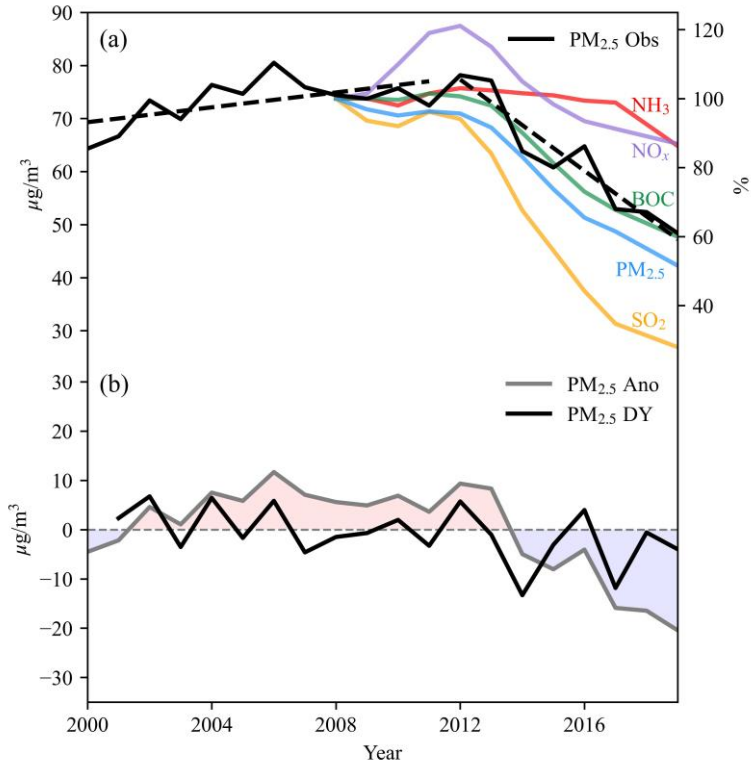
128 **3.1 Roles of emission**

129 Human activities are the major source of haze pollution in east of China (Zhang and Geng, 2020), which implies that a
130 large proportion of PM_{2.5} concentration is predictable. Particularly, the large reduction of anthropogenic emissions since
131 2013 determined the decreasing trend of winter PM_{2.5} concentration (Figure 1a). As aforementioned, the socioeconomic-
132 PM_{2.5} (i.e., SE-PM_{2.5}) isolated by CMAQ could well reflect the impacts of human activities and was a potentially effective
133 predictor for seasonal prediction of PM_{2.5} concentration. As expected, the one-variable linear regression model based on
134 anomalies of SE-PM_{2.5} successfully reproduced different slopes of trend during 2001–2007, 2008–2013 and 2014–2019, but
135 the predicted PM_{2.5} concentration varied too smoothly (Figure S1a). Furthermore, the quantities were underestimated when
136 observed PM_{2.5} concentration increased and overestimated when PM_{2.5} concentration rapidly decreased. To eliminate the
137 influence of trend shift, we calculated DY of PM_{2.5} and SE-PM_{2.5}. Compared with its anomalies, PM_{2.5} DY did not show
138 significant trend but displayed regularly oscillating characteristic (Figure 1b), and its predictability was much better (Wang
139 et al., 2008). The SP-SE model was trained by DY of SE-PM_{2.5} in each grid to predict PM_{2.5} DY. After adding the predicted
140 PM_{2.5} DY to observed PM_{2.5} in the previous year, the final PM_{2.5} concentration was obtained. The CC between predicted and
141 observed PM_{2.5} was 0.87 during 2001–2019 in the east of China. The underestimated (2001–2007) and overestimated (2014–
142 2019) values in Figure S1a were largely corrected and interannual variation also appeared in the results of SP-SE prediction
143 (Figure S1b). The staged trends from the SP-SE model almost overlapped with the observed trends, indicating the model
144 performed well in capturing the changes of trend (Figure S2).

145 North China (NC; 34–42°N, 114–120°E), the Yangtze River Delta (YRD; 27–34°N, 117–122°E) and the Pearl River
146 Delta (PRD; 21.5–25°N, 112–116°E) are three regions that have been experiencing severe PM_{2.5} pollution (Yin et al., 2015).
147 Thus, the performance of the SP-SE model in NC, the YRD and the PRD were validated separately (Table 1, Figure 2 a-c).
148 The RMSEs were 12.2, 6.2 and 6.8 µg/m³ in NC, the YRD and the PRD, respectively (Table 1). Larger RMSE in NC did not
149 indicate the SP-SE model performs worse in NC than in the YRD and the PRD, because the mean value of PM_{2.5}
150 concentration was the highest in NC. The relative bias (absolute bias/mean) in NC was 8.5%, which was smaller than that in
151 the PRD (12.9%). Consistent with its performance in east of China, the SP-SE model also well reproduced the staged trends

152 in NC, the YRD and the PRD (Figure 2 a-c). However, when the linear trend was removed, the CC between predicted and
153 observed $\text{PM}_{2.5}$ significantly decreases in all the three $\text{PM}_{2.5}$ -polluted regions (NC: from 0.78 to -0.13; YRD: from 0.88 to -
154 0.28; PRD: from 0.74 to 0.16). That is, the prediction model trained by the socioeconomic- $\text{PM}_{2.5}$ could well predict the
155 values and staged linear trends. However, it certainly had no ability to simulate the interannual variability of $\text{PM}_{2.5}$
156 concentration.

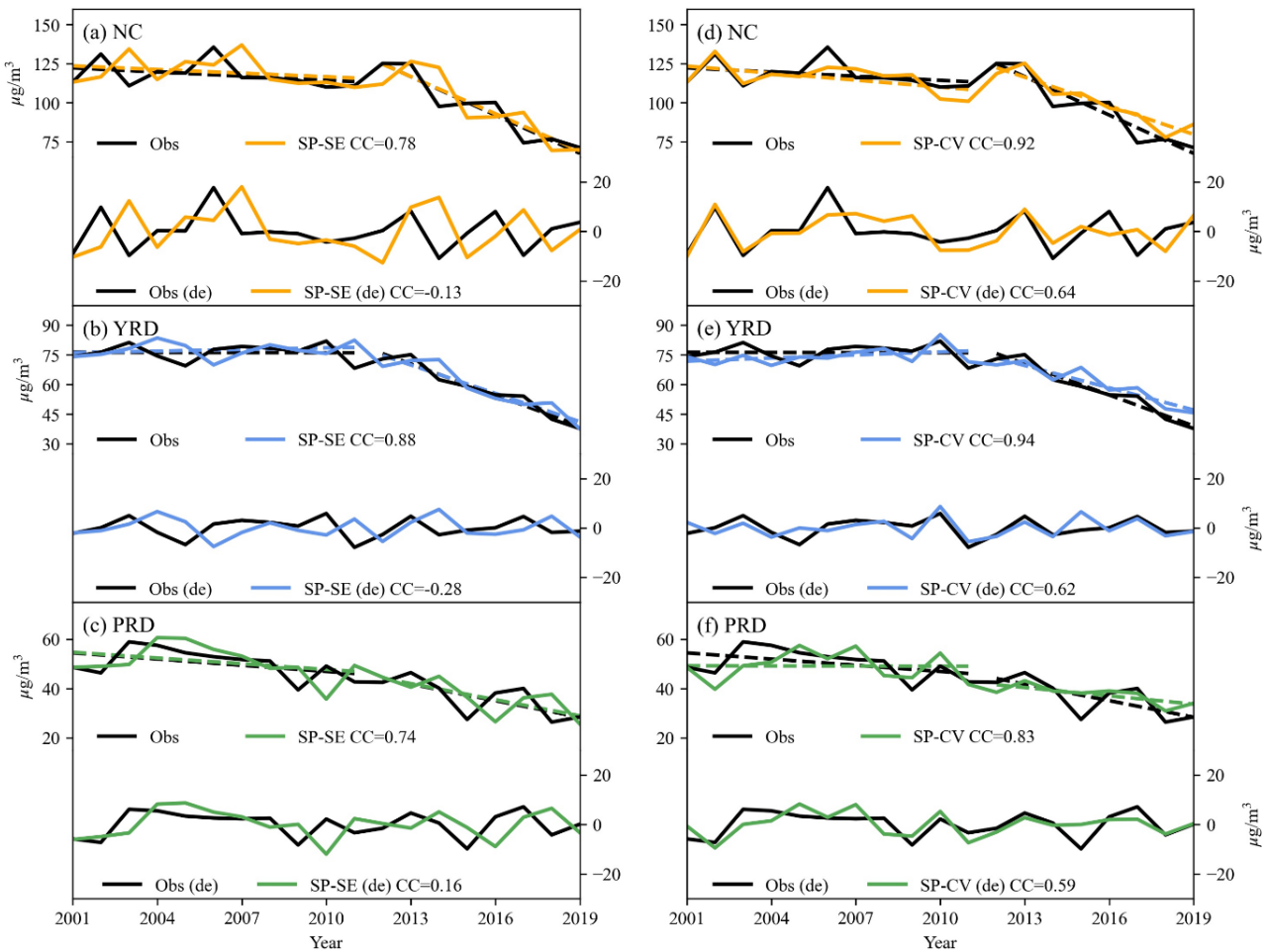


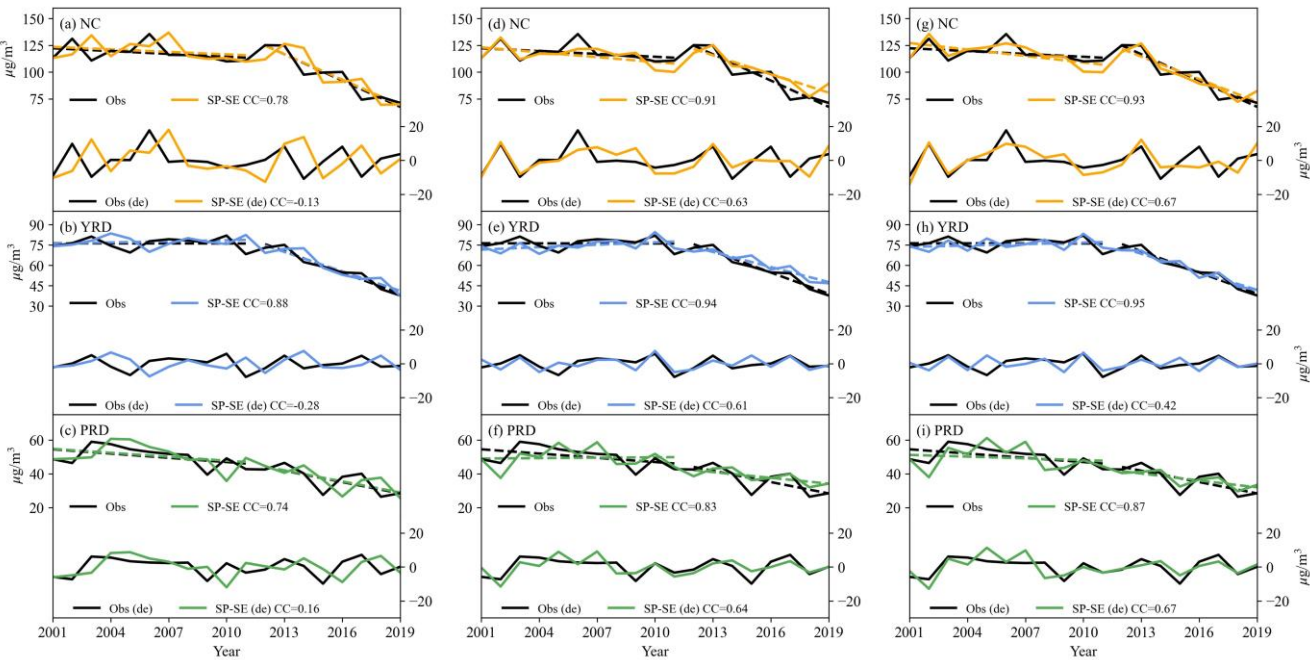


158
159 **Figure 1:** Variation in (a) winter PM_{2.5} concentration (black; unit: $\mu\text{g}/\text{m}^3$), (b) PM_{2.5} anomalies (gray; compared to the mean of
160 2000–20192020; unit: $\mu\text{g}/\text{m}^3$) and PM_{2.5} DY (black; unit: $\mu\text{g}/\text{m}^3$). Color lines in panel (a) indicate relative variations in annual
161 emissions (compared to that in 2008, unit: %) of ammonia (NH₃; red), nitrogen oxide (NO_x; purple), BOC (green), PM_{2.5} (blue),
162 and sulfur dioxide (SO₂; yellow) in east of China. The black dashed line in panel (a) indicates the linear trend of PM_{2.5}
163 concentration.

164
165 **Table 1:** The leave-one-out validated root-mean square errors (RMSE), relative biases (absolute bias mean; %) and percentages of
166 same sign (PSS) for three statistical models.

	RMSE ($\mu\text{g}/\text{m}^3$)			Relative Bias (%)		
	NC	YRD	PRD	NC	YRD	PRD
SP-SE	12.2	6.2	6.8	8.5	6.9	12.9
SP-CV	<u>7.68.0</u>	<u>4.78</u>	5.2	<u>5.23</u>	<u>5.96.2</u>	<u>9.79</u>
SP- <u>ECE</u>	<u>6.58</u>	<u>4.42</u>	<u>4.67</u>	<u>4.85.1</u>	<u>45.91</u>	<u>8.85</u>





173 **Figure 2: Variations in reanalysis (black) and SP-SE predicted winter PM_{2.5} concentration in (a) NC (orange), (b) the YRD (blue),**

174 and (c) the PRD (green) from 2001 to 2019 before (upper) and after (lower) detrending. The predicted PM_{2.5} is dependent on the

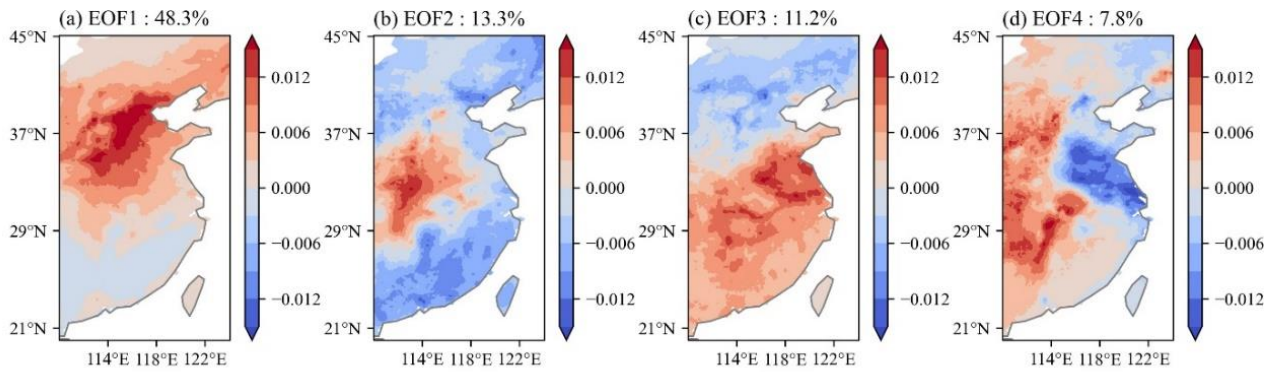
175 leave-one-out validation. (d-f) are the same as (a-c), but for SP-CV. (g-i) are the same as (a-c), but for SP-EC.

176 3.2 Impacts of climate variability

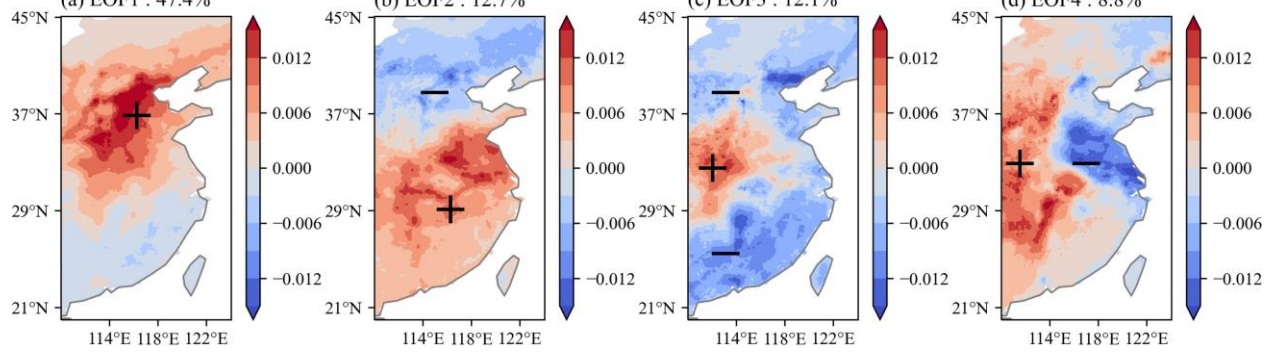
177 Decomposition and prediction of dominant modes of climate conditions were applied in short-term prediction of
 178 precipitation (Huang et al., 2022) and surface air temperature (Hsu et al., 2020) in east of China. In this study, we decompose
 179 the first four leading modes of PM_{2.5} DY during 2001-2019 (accumulated variance contribution=8^{10.5}%) produced by
 180 Empirical Orthogonal Function (EOF) analysis, built prediction model for each principal component respectively, recalculate
 181 the predicted PM_{2.5} DY by projecting the predicted PCs onto the observed EOF spatial patterns, and finally added the
 182 predicted PM_{2.5} DY to the observation in previous year to finish the development of SP-CV (Figure S3, Table S1). The
 183 interannual-decadal variation in haze pollution could be well explained by meteorological condition and preceding climate
 184 forcings (Yin et al., 2020b) such as the Arctic sea ice extent (Wang et al., 2015; Yin et al., 2019), Eurasia snow (Zou et al.,
 185 2017) and soil moisture (Yin and Wang 2018), SST in the Pacific (Yin and Wang 2016; He et al., 2019) and Atlantic (Yin
 186 and Zhang 2020a). Prediction signals from these climate anomalies could be observed before winter and owned specific
 187 physical implications.

188 The first EOF mode of PM_{2.5} DY illustrated heavily haze-polluted status in NC (Figure 3a, e). According to the
 189 correlation analysis, the September SST DY in the Southwest Pacific (CC with PC1=0.736; Figure 4a) and October SST

190 DY in the Sargasso Sea (CC=0.736; Figure 4b) were selected to be the two predictors for PC1 of PM_{2.5} DY (Table S1).
191 Both of the predictors had close relationships with dipole pattern of Eurasian cyclonic anti-cyclonic and Northeast Asian
192 cyclonic anti-cyclonic circulations (Figure S4b, c), which was identical to those associated with PC1 (Figure S4a) and could
193 restrain the invasion of induce cold air from high latitude into deviate from NC. The second EOF mode of PM_{2.5} DY showed
194 a ‘north-south’ dipole pattern (Figure 3b, f). The variations of PM_{2.5} DY in Huanghuai and the YRD accounted for a large
195 proportion. The October soil moisture DY in the Indo-China Peninsula (CC with PC23=0.73; Figure 4c) and June-August
196 SST DY in the Gulf of Alaska (CC=−0.69; Figure 4d) were selected to build prediction model of PC2 (Table S1). The
197 anomalous atmospheric circulation associated with PC2 and its predictors could enhance cold air invasion to NC (strong
198 northerlies) but prevented the cold air from moving further south (weak 10m winds in Figure S4 d-f). The second EOF mode
199 indicated a tripole pattern with centers located in the east of Inner Mongolia, the Fenwei Plain and South China, respectively
200 (Figure 3b, f). The Fenwei Plain was highly polluted and gained a great attention in recent years, while the other two centers
201 have relatively better air quality (Zhao et al., 2021). The October snow depth DY in eastern Siberia (CC with PC2=0.73;
202 Figure 4e), October sea ice DY in the north to Barents Sea (CC=0.75; Figure 4d) and September October soil moisture DY
203 in the Indian Peninsula (CC=0.84; Figure 4e) were considered in the prediction model (Table S1). The predictors possibly
204 induced atmospheric responses in winter (Figure S4 e-g) that were similar to PC2 (Figure S4 d). The anti-cyclonic anomaly
205 over the Fenwei Plain restricted horizontal and vertical dispersion of haze particles (Zhong et al., 2019).

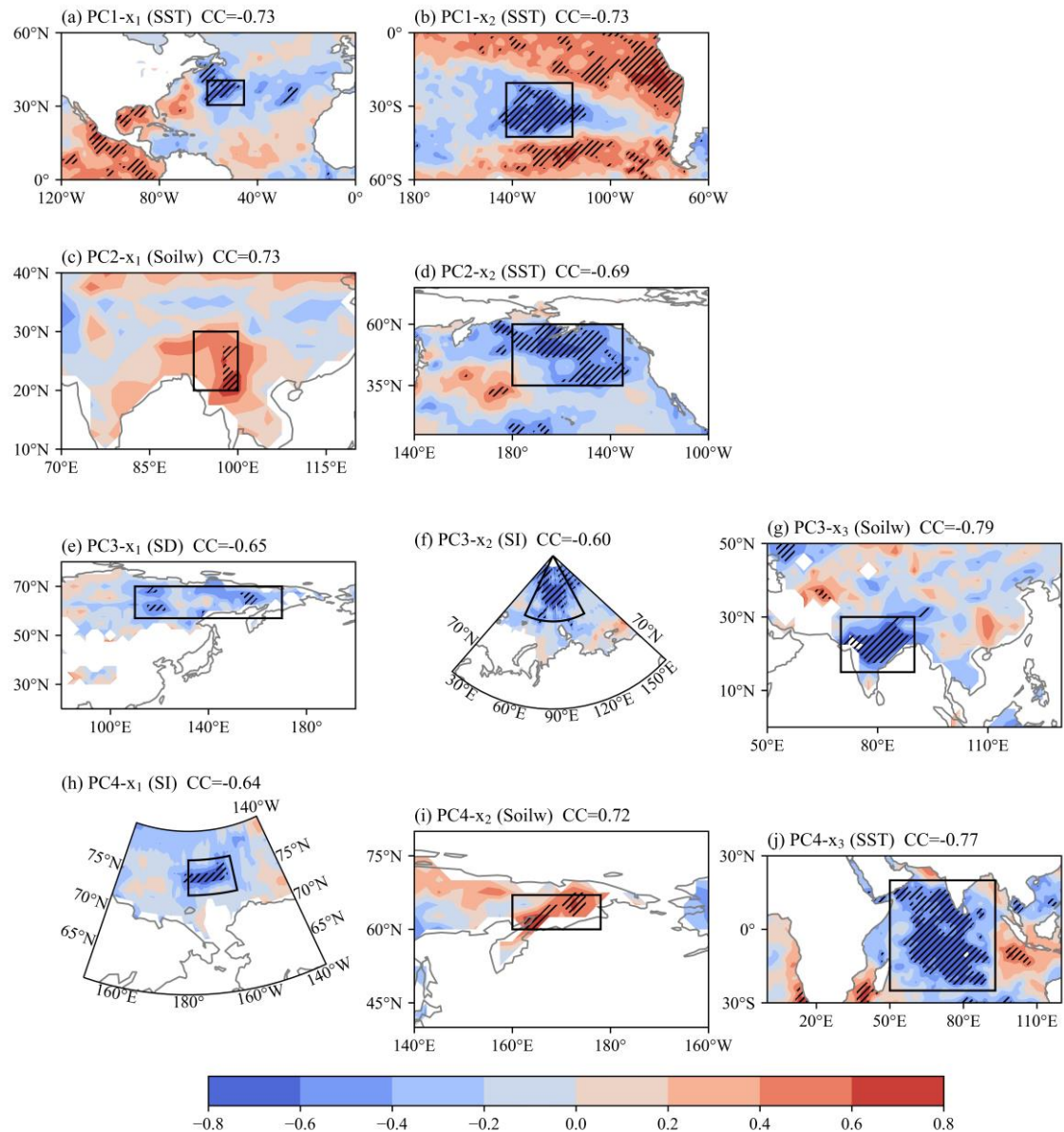


206



207

208 **Figure 3: Spatial patterns (a-d) and corresponding PCs (e-h) of the first four EOF modes for winter PM_{2.5} DY in east of China**
209 **during 2000–2019.** The variance accounted for by each EOF mode is given in the panel.



210

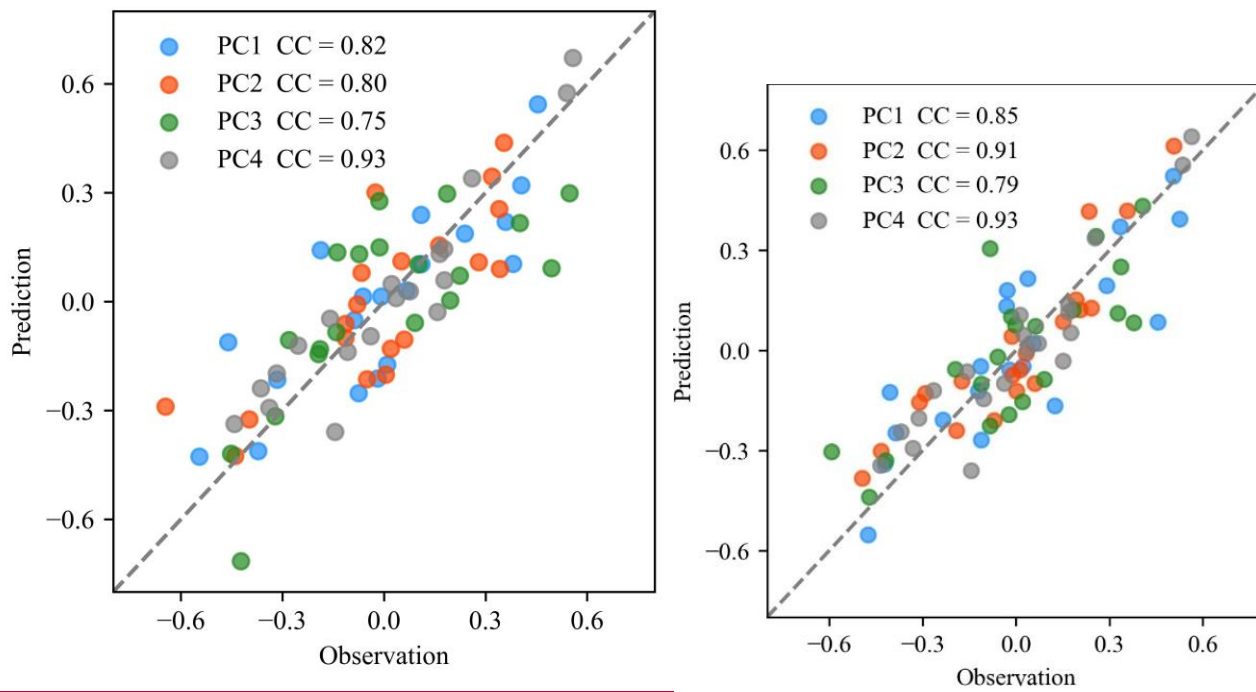
211 **Figure 4: CCs between climate predictors and (a-b) PC1, (c-ed) PC2, (ge-fg) PC3, (h-j) PC4 from 2000 to 2019.** The predictors
 212 for PC1 are (a) September SST over the South Pacific Ocean and (b) October SST over the Sargasso Sea. The predictors for PC2
 213 are (c) October Soilw over the Indo-China Peninsula and (d) June-August SST over the Gulf of Alaska. (e) October SD over
 214 eastern Siberia, (d) October SI over the Kara Sea and (e) September-October Soilw over the Indian Peninsula. The predictors for
 215 PC3 are (e) October SD over eastern Siberia, (f) October SI over the Kara Sea and (g) September-October Soilw over the Indian
 216 Peninsula. (f) October Soilw over the Indo-China Peninsula and (g) June-August SST over the Gulf of Alaska. The predictors for
 217 PC4 are (h) October SI over the Chukchi Sea, (i) October soil moisture over the Kamchatka Peninsula and (j) August-September

218 SST over the Arabian Sea and the Bay of Bengal. The slashes indicate CCs exceeding the 95% confidence level. The black boxes
219 indicate the regions over which the predictors are calculated.

220 The third EOF mode of $PM_{2.5}$ DY showed a ‘north-south’ dipole pattern (Figure 3e, g). The variations of $PM_{2.5}$ -DY in
221 Huanghuai and the YRD accounted for a large proportion. The October soil moisture DY in the Indo-China Peninsula (CC
222 with PC3=0.74; Figure 4f) and June-August SST DY in the Gulf of Alaska (CC=0.66; Figure 4g) were selected to build
223 prediction model of PC3 (Table S1). The anomalous atmospheric circulation associated with PC3 and its predictors could
224 enhance cold air invasion to NC (strong northerlies) but prevented the cold air from moving further south (weak 10m winds
225 in Figure S4 h-j). The third EOF mode indicated a triple-triplet pattern with centers located in the east of Inner Mongolia, the
226 Fenwei Plain and South China, respectively (Figure 3c, g). The Fenwei Plain was highly polluted and gained a great
227 attention in recent years, while the other two centers have relatively better air quality (Zhao et al., 2021). The October snow
228 depth DY in eastern Siberia (CC with PC3=−0.65; Figure 4e), October sea ice DY in the north to Barents Sea (CC=−0.60;
229 Figure 4f) and September-October soil moisture DY in the Indian Peninsula (CC=−0.79; Figure 4g) were considered in the
230 prediction model (Table S1). The predictors possibly induced atmospheric responses in winter (Figure S4 h-j) that were
231 similar to PC3 (Figure S4 g). The abnormal northerlies over North China and South China anti-enhanced the cyclonic
232 anomaly over the Fenwei Plain restricted horizontal and vertical dispersion of haze particles (Zhong et al., 2019), while the
233 weak wind speed and surface wind convergence in central China were conducive to the accumulation of pollutants. A
234 statistical model (Table S1) was also developed to predict the ‘East-West’ dipole shown in the fourth EOF mode (Figure 3d,
235 h) based on October sea ice DY in the Chukchi Sea (CC=−0.64; Figure 4h), October soil moisture DY in the Kamchatka
236 peninsula (CC=0.7472; Figure 4i) and August-September SST DY in the Arabian Sea (CC=−0.7677; Figure 4j). The
237 atmospheric anomalies in the lower troposphere and near surface, which were associated with the above predictors and PC4,
238 also had similar impacts on haze pollution (Figure S4 k-n).

239 As shown in Figure 5, multiple linear regression model demonstrated good performance in simulating the variation in
240 each PC. The CCs between observed and predicted 1st–4th PCs were 0.8582, 0.9180, 0.7975 and 0.93, respectively, all of
241 which were above the 99% confidence level, indicating that the model successfully reproduced each individual EOF mode.
242 Meanwhile, the yearly increment approach had the ability to address trend and its changes that were not obviously
243 mutational (Yin and Wang 2016). The CC between observed and predicted $PM_{2.5}$ concentrations before (after) detrending by
244 stages was 0.9291 (0.6463) in NC, 0.94 (0.6261) in the YRD and 0.83 (0.5964) in the PRD in the leave-one out validation
245 (Figure 2 d-f). Thus, the SP-CV model well simulated both the trend and the interannual variation of $PM_{2.5}$ concentration in
246 the east of China. In addition, the RMSEs in NC, the YRD and the PRD were 7.68.0, 4.87 and 5.23 $\mu\text{g}/\text{m}^3$ and the relative
247 biases were 5.23%, 56.2% and 59.9%, respectively (Table 1), all of which were obviously smaller than those of SP-SE. The
248 PSS, which is an important indicator of climate prediction, was also evaluated relative to the winters of 2001–2019. The
249 area-averaged PSS from SP-CV was 80.479.9% in east of China, which was 8.17.9% higher than that from SP-SE (Figure 6).
250 Although the SP-CV model performed better than the SP-SE, especially that it could capture the sharp downward trend after

251 2013 in NC and YRD, the RMSEs of the SP-CV simulations for the period 2015-2019 increased up to 11.64, 6.54 and 5.38
 252 $\mu\text{g}/\text{m}^3$ in NC, the YRD and the PRD compared to that of the SP-SE simulations. Obvious positive biases were found in the
 253 predictions of $\text{PM}_{2.5}$ concentration after 2014 (Figure 2 d-f) because the SP-CV model was short of information about the
 254 super-strict emission regulations (Figure S2). Based on different levels of haze pollution, various degrees of air pollution
 255 control were carried out in NC, the YRD and the PRD (Zhang and Geng, 2020). In NC, where anthropogenic emissions were
 256 most prominently restricted, the predicted biases were also the largest (Figure 2d). The predicted biases were the smallest in
 257 the PRD, while that in the YRD were in-between. These results were consistent with different intensities of pollution control
 258 in the three regions (Figure 2e, f), which further indicated the importance to fully take into account the impacts of climate
 259 variability and anthropogenic emissions.



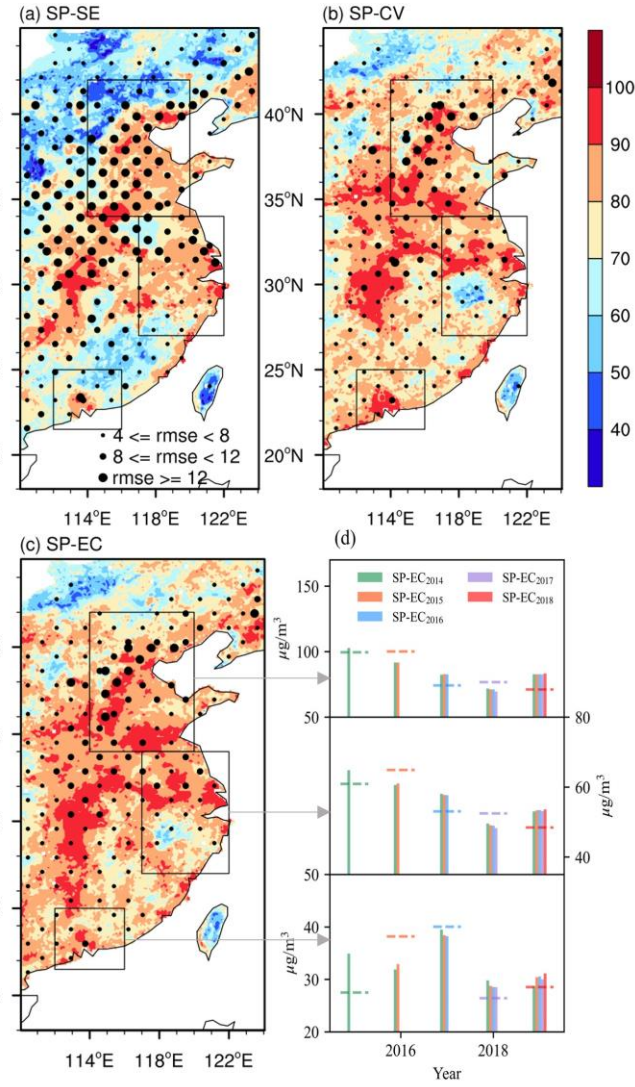
260
 261 **Figure 5: Scatter plots of normalized observed (x axis) and predicted (y axis) PC1 (blue), PC2 (red), PC3 (green) and PC4 (gray)
 262 from 2000 to 2019. The predicted PCs are dependent on the leave-one-cross validation.**

263 **4 PM_{2.5} prediction with integrated factors**

264 As aforementioned, the SP-SE model trained by the SE-PM_{2.5} DY considered the impacts of emission changes one-
 265 sidedly and could well simulate the values and staged trends. However, it completely failed to reproduce the interannual
 266 variation of winter PM_{2.5} concentration in east of China (Figure 2 a-c). Differently, the predictors of climate variability could
 267 introduce the interannual variation of winter PM_{2.5} and the yearly increment approach had the ability to bring in the slow

268 trend. The SP-CV model successfully predicted most of the trend and interannual variation in PM_{2.5} concentration (Figure 2
269 d-f) but underestimated the sharp decreasing trend (Figure S2), which led to positive forecast biases after 2013 (Figure 2d-f).

270 To fully contain predictive signals of human activities and climate anomalies, the predicted PM_{2.5} DY from SP-SE and
271 SP-CV model for the current year were added up and the sum was added to PM_{2.5} observations in the previous year to
272 develop the final prediction model, i.e., the SP-EC model. As expected, the performance of SP-EC model was better than
273 that of both SP-SE and SP-CV models. Area-averaged PSS was 81.48% in east of China (Figure 6). The CC between
274 observed and SP-EC-predicted PM_{2.5} concentrations before (after) detrending was 0.96 (0.748) in east of China; the RMSE
275 was 2.757 $\mu\text{g}/\text{m}^3$, which was 43.87% (32.53%) smaller than the RMSE of SP-SE (SP-CV) in the leave-one out validation.
276 That is, the trend simulated by the SP-EC model almost overlapped with the trend of observations (similar to results of SP-
277 SE) and the interannual variation was also reproduced (similar to results of SP-CV). The CCs between observed and SP-EC-
278 predicted PM_{2.5} concentrations before (after) detrending were 0.93 (0.678) in NC, 0.95 (0.424) in the YRD and 0.88-87
279 (0.6667) in the PRD (Figure 2g-i). The RMSEs were 6.5-8 in NC, 4.24 in YRD and 4.76 $\mu\text{g}/\text{m}^3$ in PRD, which were 446.37%
280 (154.05%), 323.39% (12.58%) and 302.94% (944.65%) smaller than that of SP-SE (SP-CV), indicating greater
281 improvements in NC than in the other two regions (Table 1). According to the relative biases, the SP-EC model also
282 demonstrated a better skill in NC (4.85.1%) than that in the YRD (4.95.1%) and the PRD (8.85%) in the leave-one out
283 validation. As shown in Figure 7, the decreases in PM_{2.5} resulted from the implementation of strict emission control
284 measures in recent years were also reproduced by the SP-EC model. The evident and positive biases in the SP-CV results
285 were largely corrected in east of China, NC, the YRD and the PRD (Figure 7).



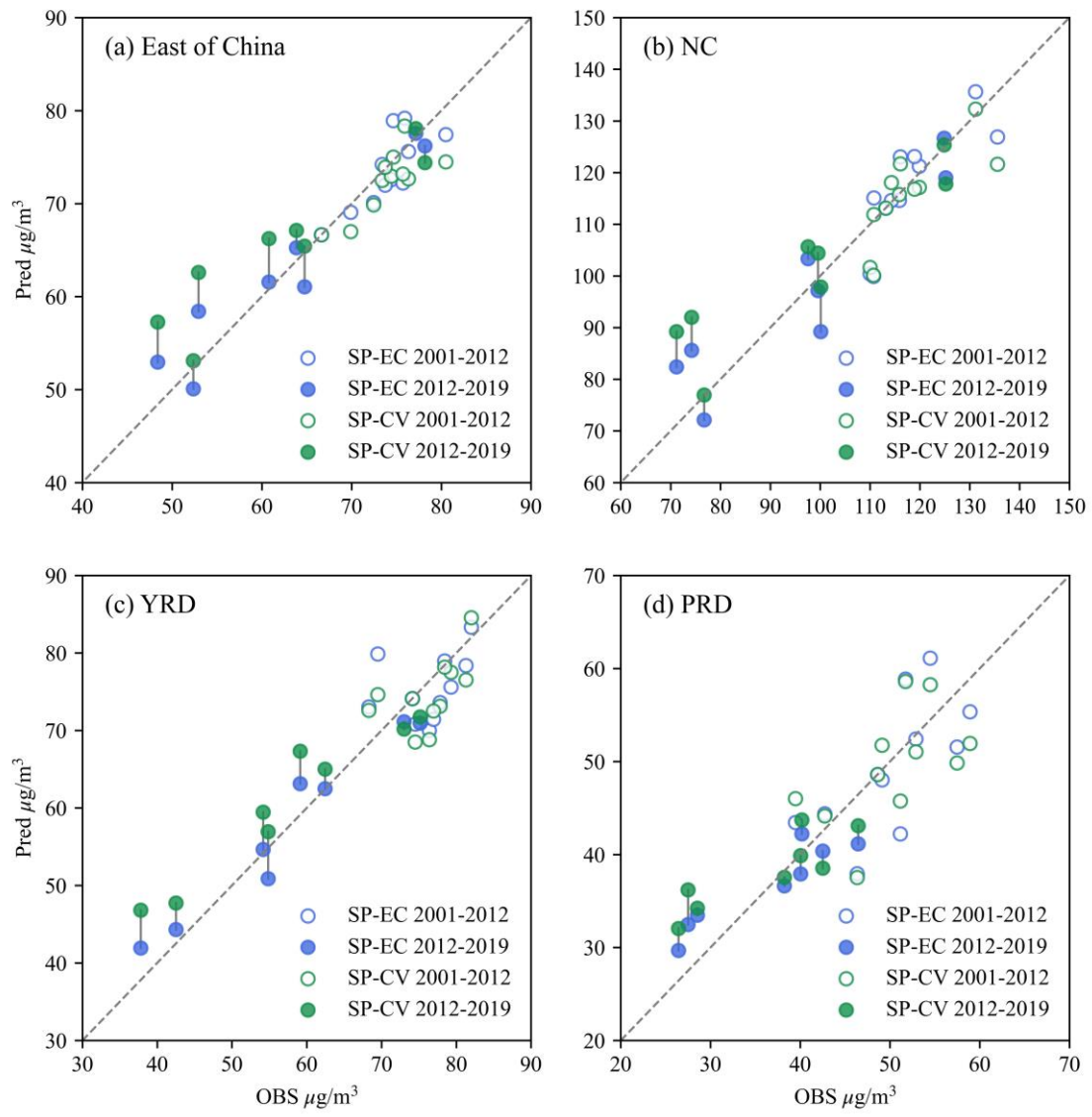
286

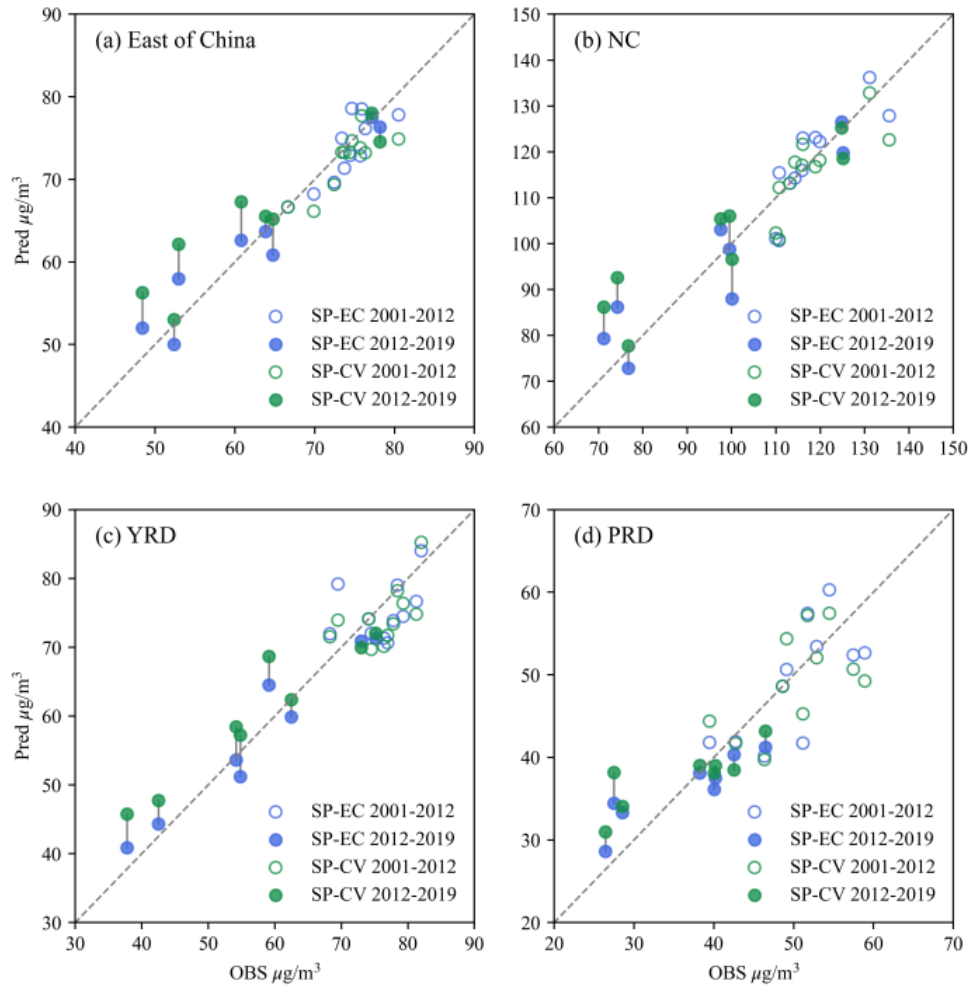
287 **Figure 6: Distributions of PSS (shadings) and RMSE (dots) from (a) SP-SE, (b) SP-CV, and (c) SP-EC. The boxes represent NC,**

288 the YRD and the PRD respectively, and the arrows point to the SP-EC predicted PM_{2.5} in recycling independent tests (bars) and

289 observations (dashed lines) corresponding to the area. The subscript in the legend of panel (d) indicates the model trained from

290 2000 to this year, and the PM_{2.5} from the next year to 2019 are independently predicted.

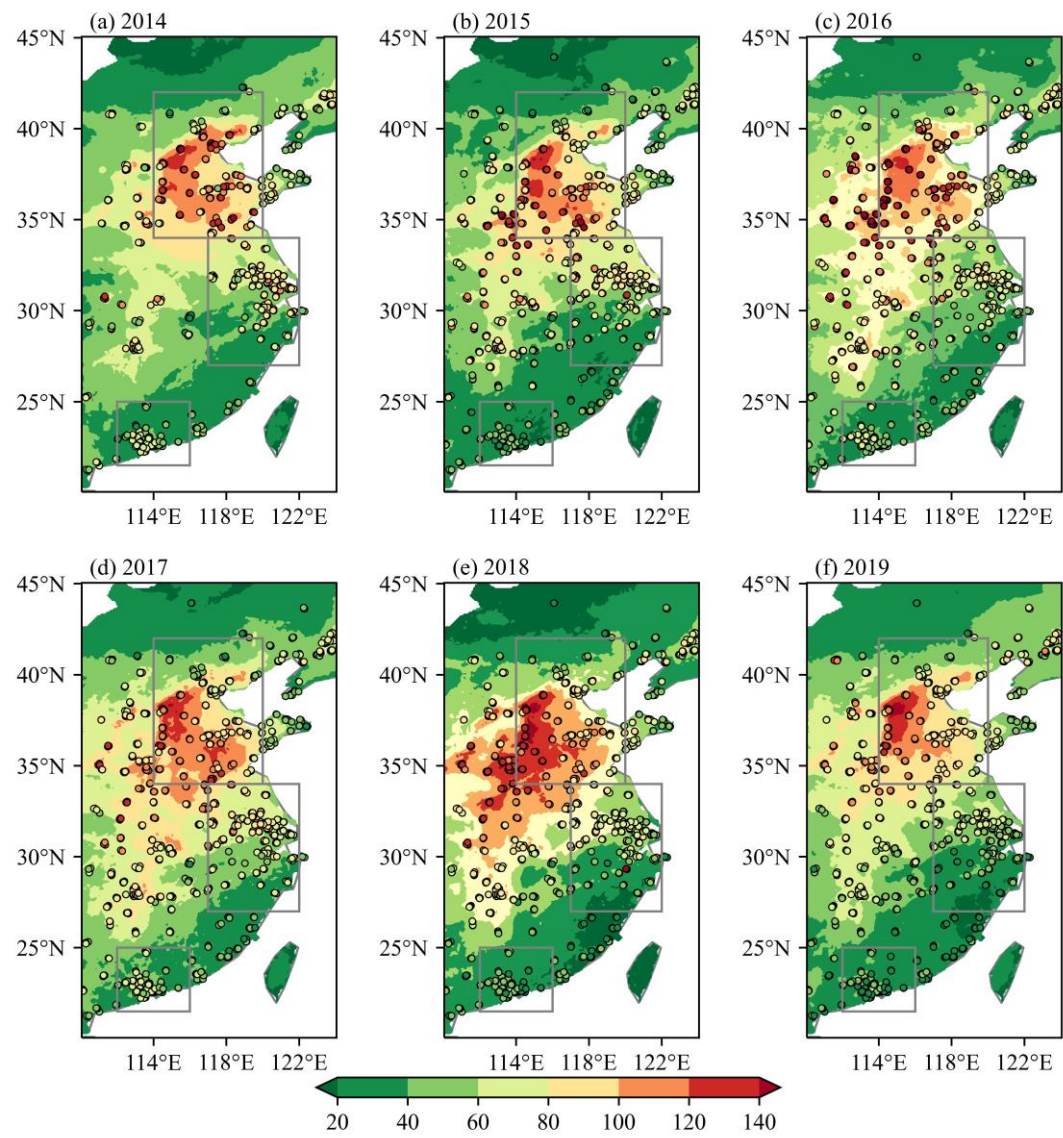


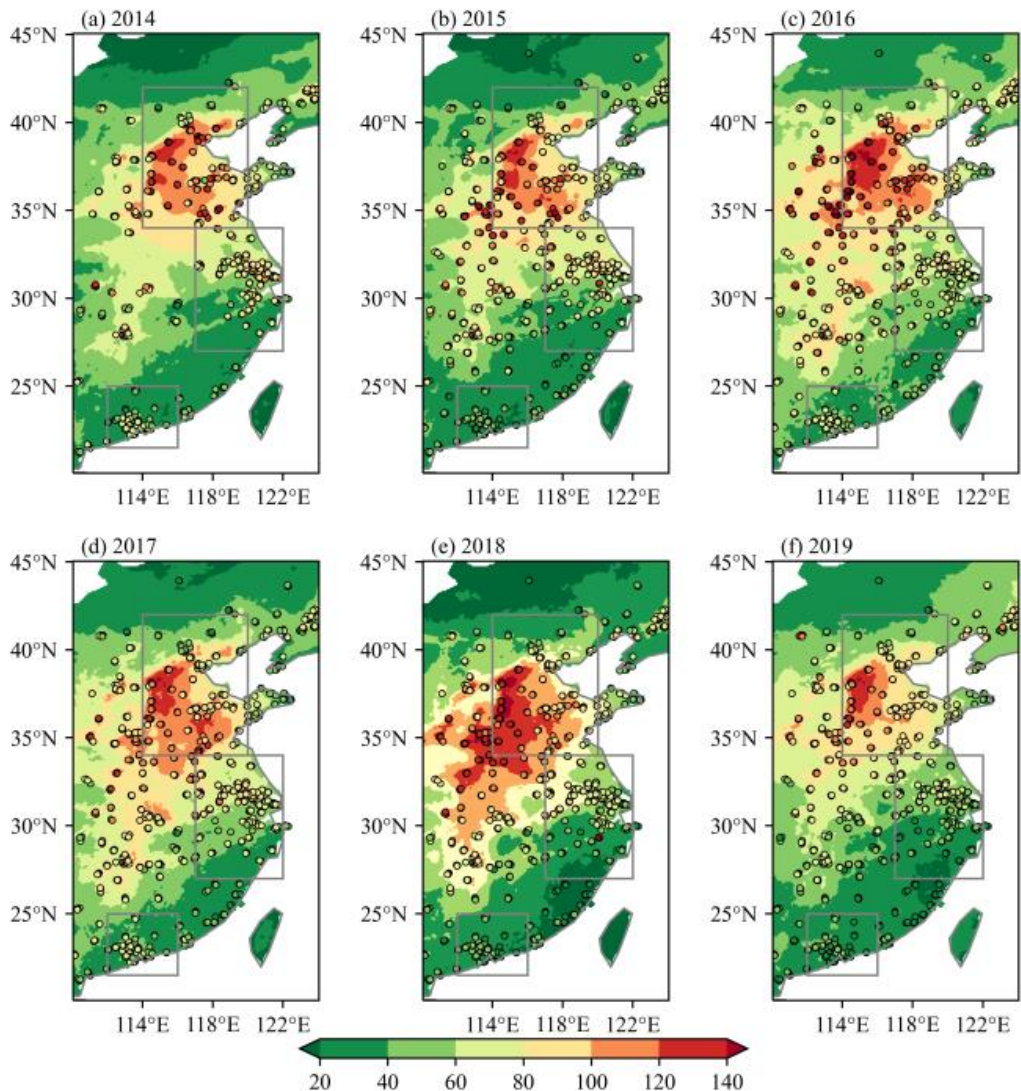


292
293 **Figure 7: Scatter plots of the reanalysis (x axis) and predictions of (y axis) PM_{2.5} concentration by SP-CV (green) and SP-EC (blue)
294 in (a) east of China, (b) NC, (c) the YRD and (d) the PRD. The points during 2012–2019 are filled and the short lines between SP-
295 CV and SP-EC pointes indicate the calibrations.**

296 High spatial resolution was one of the advantages of the seasonal prediction model developed in this study. That is, the
297 SP-EC model could predict winter PM_{2.5} concentration at each 10km×10km grid in east of China. When only considering
298 emission predictors (i.e., SP-SE), RMSEs>12 $\mu\text{g}/\text{m}^3$ were found in middle part of the study region and the PSS was lower
299 than 60% in South China and the Inner Mongolia (Figure 6a). When only considering climate predictors (i.e., SP-CV),
300 RMSEs>12 $\mu\text{g}/\text{m}^3$ existed in Beijing and its surrounding areas and PSS significantly increased compared to the result of SP-
301 SE (Figure 6b). When integrating both of the emission predictors and climate predictors (i.e., SP-EC), the RMSE in each
302 grid further decreased and the PSS also increased (Figure 6c). In middle part of the study region, the PSS was higher than
303 80%. In view of gaps between site observations and model simulations, the SP-EC-predicted PM_{2.5} concentrations were

304 compared with site observations (Figure 8). NC was the most severely polluted area and the SP-EC model could capture the
305 PM_{2.5} values and interannual differences. Particularly, the SP-EC model reproduced the sudden rebound of PM_{2.5} pollution in
306 2018 (Figure 8e) that was mainly resulted from climate anomalies (Yin and Zhang 2020a). ~~However, the model failed to~~
307 ~~well predict the evident PM_{2.5} drops in east of China (Figure 8f) caused by COVID-19 quarantines (Yin et al., 2021).~~





309
 310 **Figure 8: SP-EC predicted (shading) and site-observed (scatter) PM_{2.5} concentrations (units: $\mu\text{g}/\text{m}^3$) in (a) 2014, (b) 2015, (c) 2016,
 311 (d) 2017, (e) 2018 and (f) 2019. The boxes represent NC, the YRD and the PRD respectively.**

312 Due to the limitation of short sequence of data, recycling independent tests (RIT) were designed to further verify the
 313 performance of the SP-EC model. In the RIT predictions, the prediction model was trained by samples from 2001 to the
 314 expiration year of training data and the PM_{2.5} anomalies from the next year to 2019 were independently predicted. For
 315 example, the prediction model trained by the data from 2001 to 2014 can produce independent predictions from 2015 to
 316 2019. The expiration year of the training data moved forward from 2015 to 2019, so there were 15 independent predictions.
 317 The PM_{2.5} concentration was independently predicted 5 times for 2019, 4 times for 2018, and so on. The PSS of PM_{2.5}
 318 anomalies was 100%, not only relative to winters of 2001–2019 but also 2015–2019, indicating a high accuracy of prediction

319 in east of China. The predicted values for each year did not vary much (Figure 6d), indicating a high reliability and
320 robustness of the model. For example, when the SP-EC model was trained by the samples only from 2000 to 2014, the
321 predicted PM_{2.5} anomalies for 2018 and 2019 were also close to the results of leave-one-out validations and the
322 measurements.

323 5 Conclusions and discussion

324 The change of haze pollution consisted of long-term trend, interannual-decadal variations, synoptic disturbances and so
325 on. Seasonal prediction ~~was~~ focused on predicting long-term trend and interannual-decadal variations 1~3 months in advance
326 (Wang et al., 2021). Because of the limitation of short observational period, many previous studies employed the number of
327 haze days as proxy of PM_{2.5} pollution to build statistical prediction model (Yin and Wang 2016; Yin et al., 2017; Dong et al.,
328 2021; Zhao et al., 2021; Chang et al., 2021). Since 2020, several high-resolution PM_{2.5} reanalysis datasets have been
329 successively released, which greatly increased the possibility for direct seasonal prediction of PM_{2.5} concentration that is
330 more familiar to decision makers and the public (Yin et al., 2021).

331 In this study, two seasonal prediction models were separately trained by emission factor (i.e., SP-SE) or preceding
332 climate predictors (i.e., SP-CV) to discuss their relative contributions. The SP-SE model could simulate the slow rising trend
333 of PM_{2.5} concentration before 2012 and the strong downward trend after 2012. However, it was incapable of importing the
334 interannual component. The SP-CV model benefited from the year-to-year increment approach and could introduce a large
335 portion of the linear trend except the sharp decrease of winter PM_{2.5} concentration from 2013. Furthermore, the SP-CV
336 model performed well in predicting the obvious interannual variation of PM_{2.5} concentration. We integrated the emission and
337 climate factors to establish the final prediction model (i.e., SP-EC), which could well reproduce both the trend and the
338 interannual variation of PM_{2.5} concentration. The area-averaged PSS was 81.~~84~~ % in east of China and CC between observed
339 and predicted PM_{2.5} concentrations before (after) the detrending was 0.96 (0.7~~48~~). The RMSEs were 6.~~85~~ in NC, 4.~~24~~ in the
340 YRD and 4.~~76~~ $\mu\text{g}/\text{m}^3$ in the PRD, which were 44.3% (15.0%), 32.3% (12.5%) and 30.9% (9.6%) 46.7% (14.5%), 33.9%
341 (12.8%) and 32.4% (11.5%) smaller than that the results of SP-SE (SP-CV). Due to the implementation of the super-strict
342 emission control measures, the air quality has been substantially improved and this improvement was also perfectly
343 predicted by the SP-EC model. During recycling independent tests, the PSS of PM_{2.5} anomalies was 100%, demonstrating
344 high accuracy and robustness. The high-resolution PM_{2.5} prediction could provide scientific supports for air pollution control
345 at the regional and city levels. Considering the severe impact of haze pollution For example, real-time PM_{2.5} climate
346 prediction is highly demanded for the purpose to determine how to reduce anthropogenic emissions and how much should
347 be reduced; 10km \times 10km gridded PM_{2.5} information also had potentials to support finely and dynamically regional
348 managements and collaborations.

349 This study mainly focused on ~~the developments~~ of seasonal PM_{2.5} prediction model. The Related theories and methods

350 ~~for seasonal prediction of PM_{2.5} concentration are still exploratory and need further discoveries.~~ Although the SP-EC model

351 was proved to be skilled, the underlying physical mechanisms of climate predictors were not sufficiently explained and

352 needed further in-deep studies. As shown in Figure 8f, the SP-EC model failed to well predict the evident PM_{2.5} drops in east

353 of China caused by COVID-19 quarantines in the winter of 2019 (especially February in 2020) (Yin et al., 2021). Therefore,

354 such sudden fluctuations of PM_{2.5} concentration were not involved in the established prediction model. Furthermore, the

355 EOF pattern of PM_{2.5} possibly changed under climate change and must influence the climate component of PM_{2.5}, which

356 should be updated in time. Furthermore, although ~~Although~~ the SP-EC model had high spatial resolution, it could only output

357 winter-mean PM_{2.5} concentration. It was meaningful to build monthly sub-seasonal models to provide more detailed

358 predictions. In addition, modern weather and climate forecasts were heavily dependent on numerical prediction models.

359 Thus, it is imperative to design and develop numerical models that target at routine seasonal prediction of air pollution (Yin

360 et al., 2021). The theories and methods for seasonal prediction of PM_{2.5} concentration are still exploratory and need further

361 discoveries. Considering the severe impact of haze pollution, real-time climate prediction is highly demanded for the purpose

362 to determine how to reduce anthropogenic emissions and how much should be reduced.

363 Data availability

364 The monthly sea ice concentration and sea surface temperature (SST) dataset were provided by the Met Office Hadley

365 Centre: <https://www.metoffice.gov.uk/hadobs/hadisst/> (Rayner et al. 2003). Monthly soil moisture, snow depth, geopotential

366 height at 500hPa and 850hPa, sea level pressure and 10m wind were extracted from the fifth generation reanalysis product

367 (ERA5) produced by the European Center for Medium Range Weather Forecasts:

368 <https://cds.climate.copernicus.eu/#!/search?text=ERA5&type=dataset> (Hersbach et al. 2020). Annual emissions of ammonia,

369 nitrogen oxide, BOC, primary PM_{2.5}, and sulfur dioxide in China were derived from the MEIC model:

370 <http://www.meicmodel.org/> (Li et al., 2017). Hourly site-observed PM_{2.5} concentration during 2014–2019 were acquired

371 from the China National Environmental Monitoring Centre: <https://www.aqistudy.cn/historydata/> (CNEMC, 2021). The

372 long-term and high-resolution TAP PM_{2.5} concentration dataset during 2000–2019 can be downloaded from

373 <http://tapdata.org> (Geng et al. 2021b).

374 Authors' contribution

375 Wang H. J. and Yin Z. C. designed this research. Li Y. Y., Xu T. B. and Duan M. K. performed analyses and trained

376 prediction models. Yin Z. C. prepared the manuscript with contributions from all co-authors.

377 **Competing interests**

378 The authors declare no conflict of interest.

379 **Acknowledgements**

380 This research is supported by the National Natural Science Foundation of China (No. 42088101).

381 **References**

382 An, J., Chen, Y., Qu, Y., Chen, Q., Zhuang, B., Zhang, P., and Wu, Q.: An online-coupled unified air quality forecasting
383 model system, China, *Adv. Earth Sci.*, 33, 445–454, <https://doi.org/10.11867/j.issn.1001-8166.2018.05.0445>, 2018.

384 Chang, L., Wu, Z., and Xu, J.: Contribution of Northeastern Asian stratospheric warming to subseasonal prediction of the
385 early winter haze pollution in Sichuan Basin, China, *Sci Total Environ*, 751, 141823,
386 <https://doi.org/10.1016/j.scitotenv.2020.141823>, 2021.

387 Cheng, X. G., Boiyo, R., Zhao, T. L., Xu, X. D., Gong, S. L., Xie, X. N., and Shang, K.: Climate modulation of Niño3.4
388 SST-anomalies on air quality change in southern China: Application to seasonal forecast of haze pollution, *Atmos. Res.*, 225,
389 157–164, <https://doi.org/10.1016/j.atmosres.2019.04.002>, 2019.

390 Cohen, A. J., Brauer, M., Burnett, R., Anderson, H. R., Frostad, J., Estep, K., Balakrishnan, K., Brunekreef, B., Dandona, L.,
391 Dandona, R., Feigin, V., Freedman, G., Hubbell, B., Jobling, A., Kan, H., Knibbs, L., Liu, Y., Martin, R., Morawska, L.,
392 Pope, C. A., Shin, H., Straif, K., Shaddick, G., Thomas, M., van Dingenen, R., van Donkelaar, A., Vos, T., Murray, C. J. L.,
393 and Forouzanfar, M. H.: Estimates and 25-year trends of the global burden of disease attributable to ambient air pollution: an
394 analysis of data from the Global Burden of Diseases Study 2015, *The Lancet*, 389, 1907–1918,
395 [https://doi.org/10.1016/s0140-6736\(17\)30505-6](https://doi.org/10.1016/s0140-6736(17)30505-6), 2017.

396 Dong, Y., Yin, Z. C., and Duan, M. K.: Seasonal prediction of winter haze days in the Yangtze River Delta, China,
397 *Transactions of Atmospheric Sciences*, 44, 290–301, <https://doi.org/10.13878/j.cnki.dqkxxb.20200525001>, 2021.

398 Dun, M., Xu, Z., Wu, L., and Yang, Y.: Predict the particulate matter concentrations in 128 cities of China, *Air. Qual. Atmos.*
399 *Hlth.*, 13, 399-407, <https://doi.org/10.1007/s11869-020-00819-5>, 2020.

400 Gao, M., Sherman, P., Song, S., Yu, Y., Wu, Z., and McElroy, M. B.: Seasonal prediction of Indian wintertime aerosol
401 pollution using the ocean memory effect, *Science Advances*, 5, eaav4157, <https://doi.org/10.1126/sciadv.aav4157>, 2019.

402 Geng, G., Zheng, Y., Zhang, Q., Xue, T., Zhao, H., Tong, D., Zheng, B., Li, M., Liu, F., Hong, C., He, K., and Davis, S. J.:
403 Drivers of PM2.5 air pollution deaths in China 2002–2017, *Nat. Geosci.*, 14, 645-650, <https://doi.org/10.1038/s41561-021->

404 00792-3, 2021a.

405 Geng, G., Xiao, Q., Liu, S., Liu, X., Cheng, J., Zheng, Y., Xue, T., Tong, D., Zheng, B., Peng, Y., Huang, X., He, K., and
406 Zhang, Q.: Tracking Air Pollution in China: Near Real-Time PM2.5 Retrievals from Multisource Data Fusion, *Environ. Sci.*
407 *Technol.*, 55, <https://doi.org/10.1021/acs.est.1c01863>, 2021b.

408 He, C., Liu, R., Wang, X. M., Liu, S. C., Zhou, T. J., and Liao, W. H.: How does El Nino-Southern Oscillation modulate the
409 interannual variability of winter haze days over eastern China?, *Sci. Total. Environ.*, 651, 1892–1902,
410 <https://doi.org/10.1016/j.scitotenv.2018.10.100>, 2019.

411 Hersbach, H., Bell, B., Berrisford, P., Hirahara, S., Horányi, A., Muñoz-Sabater, J., Nicolas, J., Peubey, C., Radu, R.,
412 Schepers, D., Simmons, A., Soci, C., Abdalla, S., Abellán, X., Balsamo, G., Bechtold, P., Biavati, G., Bidlot, J., Bonavita,
413 M., Chiara, G., Dahlgren, P., Dee, D., Diamantakis, M., Dragani, R., Flemming, J., Forbes, R., Fuentes, M., Geer, A.,
414 Haimberger, L., Healy, S., Hogan, R. J., Hólm, E., Janisková, M., Keeley, S., Laloyaux, P., Lopez, P., Lupu, C., Radnoti, G.,
415 Rosnay, P., Rozum, I., Vamborg, F., Villaume, S., and Thépaut, J. N.: The ERA5 global reanalysis, *Q. J. Roy. Meteor. Soc.*,
416 146, 1999–2049, <https://doi.org/10.1002/qj.3803>, 2020.

417 Hsu, P.-c., Zang, Y., Zhu, Z., and Li, T.: Subseasonal-to-seasonal(S2S) prediction using the spatial-temporal projection model
418 (STPM), *China, Transactions of Atmospheric Sciences*, 43, 212–224, <https://doi.org/10.13878/j.cnki.dqkxxb.20191028002>,
419 2020.

420 Huang, Y. Y., Wang, H. J., Zhang, P. Y.: A skillful method for precipitation prediction over eastern China, *Atmospheric and*
421 *Oceanic Science Letters*, 15 (1): 100133, <https://doi.org/10.1016/j.aosl.2021.100133>, 2022.

422 Li, M., Liu, H., Geng, G., Hong, C., Liu, F., Song, Y., Tong, D., Zheng, B., Cui, H., Man, H., Zhang, Q., and He, K.:
423 Anthropogenic emission inventories in China: a review, *Natl. Sci. Rev.*, 4, 834–866, <https://doi.org/10.1093/nsr/nwx150>,
424 2017.

425 Rayner, N. A., Parker, D. E., Horton, E. B., Folland, C. K., Alexander, L. V., Rowell, D. P., Kent, E. C., and Kaplan, A.:
426 Global analyses of sea surface temperature, sea ice, and night marine air temperature since the late nineteenth century. *J.*
427 *Geophys. Res.*, 108, 4407, <https://doi.org/10.1029/2002JD002670>, 2003.

428 Wang, H. J., Chen, H. P., and Liu, J. P.: Arctic sea ice decline intensified haze pollution in eastern China, *Atmospheric and*
429 *Oceanic Science Letters*, 8, 1–9, <https://doi.org/10.3878/AOSL20140081>, 2015.

430 Wang, H., Dai, Y., Yang, S., Li, T., Luo, J., Sun, B., Duan, M., Ma, J., Yin, Z., and Huang, Y.: Predicting climate anomalies:
431 A real challenge, *Atmospheric and Oceanic Science Letters*, <https://doi.org/10.1016/j.aosl.2021.100115>, 2021.

432 Wang, J. and Du, P.: Quarterly PM2.5 prediction using a novel seasonal grey model and its further application in health
433 effects and economic loss assessment: evidences from Shanghai and Tianjin, *China, Nat. Hazards*, 107, 889–909,

434 https://doi.org/10.1007/s11069-021-04614-y, 2021.

435 Wang, H., Sun, J., Lang, X.: Some New Results in the Research of the Interannual Climate Variability and Short-Term
436 Climate Prediction, China, *Chinese Journal of Atmospheric Sciences*, 32, 806–814, 2008.

437 World Health Organization: global air quality guidelines: particulate matter (PM2.5 and PM10), ozone, nitrogen dioxide,
438 sulfur dioxide and carbon monoxide, <https://apps.who.int/iris/handle/10665/345329>, 2021.

439 Wu, J., Shi, Y., Asweto, C. O., Feng, L., Yang, X., Zhang, Y., Hu, H., Duan, J., and Sun, Z.: Fine particle matters induce
440 DNA damage and G2/M cell cycle arrest in human bronchial epithelial BEAS-2B cells, *Environ Sci Pollut Res Int*, 24,
441 25071-25081, <https://doi.org/10.1007/s11356-017-0090-3>, 2017.

442 Wu, L. F., Li, N., and Zhao, T.: Using the seasonal FGM(1,1) model to predict the air quality indicators in Xingtai and
443 Handan, *Environ Sci Pollut Res Int*, 26, 14683-14688, <https://doi.org/10.1007/s11356-019-04715-z>, 2019.

444 Xiao, Q., Zheng, Y., Geng, G., Chen, C., Huang, X., Che, H., Zhang, X., He, K., and Zhang, Q.: Separating emission and
445 meteorological contributions to long-term PM2.5 trends over eastern China during 2000–2018, *Atmos. Chem. Phys.*, 21,
446 9475-9496, <https://doi.org/10.5194/acp-21-9475-2021>, 2021.

447 Xiong, P., Yan, W., Wang, G., and Pei, L.: Grey extended prediction model based on IRLS and its application on smog
448 pollution, *Appl. Soft Comput.*, 80, 797-809, <https://doi.org/10.1016/j.asoc.2019.04.035>, 2019.

449 Xu, X., Zhao, T., Liu, F., Gong, S. L., Kristovich, D., Lu, C., Guo, Y., Cheng, X., Wang, Y., and Ding, G.: Climate
450 modulation of the Tibetan Plateau on haze in China, *Atmos. Chem. Phys.*, 16, 1365-1375, <https://doi.org/10.5194/acp-16-1365-2016>, 2016.

452 Yin, Z. C. and Wang, H. J.: Seasonal prediction of winter haze days in the north central North China Plain, *Atmos. Chem.*
453 *Phys.*, 16, 14843–14852, <https://doi.org/10.5194/acp-16-14843-2016>, 2016.

454 Yin, Z. C. and Wang, H. J.: Statistical Prediction of Winter Haze Days in the North China Plain Using the Generalized
455 Additive Model, *J. Appl. Meteorol. Clim.*, 56, 2411–2419, <https://doi.org/10.1175/jamc-d-17-0013.1>, 2017.

456 Yin, Z. C. and Wang, H. J.: The relationship between the subtropical Western Pacific SST and haze over North-Central North
457 China Plain, *Int. J. Climatol.*, 36, 3479-3491, <https://doi.org/10.1002/joc.4570>, 2016.

458 Yin, Z. C. and Wang, H. J.: The strengthening relationship between Eurasian snow cover and December haze days in central
459 North China after the mid-1990s, *Atmos. Chem. Phys.*, 18, 4753–4763, <https://doi.org/10.5194/acp-18-4753-2018>, 2018.

460 Yin, Z. C. and Zhang, Y. J.: Climate anomalies contributed to the rebound of PM2.5 in winter 2018 under intensified regional
461 air pollution preventions, *Sci Total Environ*, 726, 138514, <https://doi.org/10.1016/j.scitotenv.2020.138514>, 2020a.

462 Yin, Z. C., Li, Y. Y., and Wang, H. J.: Response of early winter haze in the North China Plain to autumn Beaufort sea ice,

463 Atmos. Chem. Phys., 19, 1439–1453, <https://doi.org/10.5194/acp-19-1439-2019>, 2019.

464 Yin, Z. C., Wang, H. J., Liao, H., Fan, K., and Zhou, B. T.: Seasonal to interannual prediction of air pollution in China:
465 Review and insight, Atmospheric and Oceanic Science Letters, 100131, <https://doi.org/10.1016/j.aosl.2021.100131>, 2022.

466 Yin, Z. C., Wang, H. J., and Guo, W. L.: Climatic change features of fog and haze in winter over North China and Huang-
467 Huai Area, China, Sci. China Earth Sci., 58, 1370–1376, <https://doi.org/10.1007/s11430-015-5089-3>, 2015.

468 Yin, Z. C., Zhang, Y. J., Wang, H. J., and Li, Y. Y.: Evident PM2.5 drops in the east of China due to the COVID-19
469 quarantine measures in February, Atmos. Chem. Phys., 21, 1581–1592, <https://doi.org/10.5194/acp-21-1581-2021>, 2021.

470 Yin, Z. C., Zhou, B. T., Chen, H. P., and Li, Y. Y.: Synergetic impacts of precursory climate drivers on interannual-decadal
471 variations in haze pollution in North China: A review, Sci. Total Environ., 755, 143017,
472 <https://doi.org/10.1016/j.scitotenv.2020.143017>, 2020b.

473 Zhang, Q., Yin, Z. C., Xi, L., and co-authors.: Synergistic Roadmap of Carbon Neutrality and Clean Air for China 2021,
474 Environmental Science and Ecotechnology, Under Review, 2022.

475 Zhang, Q. and Geng, G. N.: Impact of clean air action on PM2.5 pollution in China, Sci. China Earth Sci., 62, 1845–1846,
476 <https://doi.org/10.1007/s11430-019-9531-4>, 2020.

477 Zhao, Z., Liu, S. C., Liu, R., Zhang, Z., Li, Y., Mo, H., Wu, Y.: Contribution of climate/meteorology to winter haze pollution
478 in the Fenwei Plain, China, Int. J. Climatol., 41, 4987–5002. <https://doi.org/10.1002/joc.7112>, 2021.

479 Zou, Y. F., Wang, Y. H., Zhang, Y. Z., and Koo, J.-H.: Arctic sea ice, Eurasia snow, and extreme winter haze in China,
480 Science Advances, 3, e1602751, <https://doi.org/10.1126/sciadv.1602751>, 2017.